nature communications

Article

https://doi.org/10.1038/s41467-026-68468-3

Rigid ionic-bonding networks boosting organic room temperature phosphorescence

Received: 10 July 2025

Accepted: 7 January 2026

Published online: 26 January 2026

Check for updates

Wenpeng Ye[1,2], Chao Huang[2], Anqi Lv[2], Yanhua Gao[2], Yanfei Li[1], Huili Ma[2], Zhengong Meng[2], Huifang Shi[2], Long Gu[3] ✉, Zhongfu An[2] ✉ & Wei Huang[1,2,3] ✉

Ionic bonds possess excellent advantages in organic phosphorescence enhancement due to their intense electrostatic interactions, non-directional, and unsaturated characteristics. Nowadays, host-guest doping is the mainstream strategy for synthesizing room-temperature phosphorescent materials. While this strategy may suffer from compatible molecular configurations between host and guest, it needs precise molecular design and synthesis. Herein, ionic alkyl chain molecules are selected as hosts to prepare ionic phosphorescent materials handily. The host materials are suitable for diverse guests, simply attaching quaternary ammonium groups to chromophores. By altering the isolated chromophores, diverse phosphorescence colors from blue to orange-red can be emitted with long-lived lifetimes up to 572.27 ms. Consecutive ionic bonds can be formed in host-guest materials to construct ionic-bonding networks, thereby effectively restricting the movement of guest molecules and minimizing non-radiative transitions. Notably, the matching principle of the alkyl chain in the ionic host-guest system not only provides an ordered and rigid environment but also stimulates the external heavy-atom effect effectively, thus riveting chromophores for shining phosphorescence. This strategy, through the synergistic effects of host-guest doping and ionic-bonding networks, provides a reference for studying isolated-molecular phosphorescence with non-conjugated hosts.

Organic room-temperature phosphorescence (RTP), an extraordinary optical phenomenon resulting from the radiative transition of triplet excitons in purely organic materials, has garnered significant attention due to its excellent advantages. These include prolonged emission lifetimes[1], high exciton utilization efficiencies[2], and diverse excited-state properties[3], which enable broad applications in fields such as information encryption[4], afterglow displays[5], organic light-emitting diodes (OLEDs)[6], and biological imaging[7]. Despite this potential, realizing RTP in organic materials remains a significant challenge. Weak spin-orbital coupling limits intersystem crossing (ISC) between singlet and triplet states, leading to inefficient triplet exciton generation. Furthermore, the molecular motions at room temperature often result in non-radiative decay of excitons, making it challenging to stabilize triplet excitons and achieve RTP[8]. To address these challenges, various strategies have been proposed. Enhancing spin-orbital coupling through the introduction of heavy atoms[9,10], carbonyl groups[11], and heteroatoms[12] into organic chromophores has been a primary focus. Simultaneously, strategies such as crystal engineering[13,14], host-guest doping[15,16], self-assembly[17,18], polymerization[19,20], and other approaches[21–23] have been employed to

[1]State Key Laboratory of Flexible Electronics (LoFE), Institute of Advanced Materials (IAM), School of Chemistry and Life Sciences, Nanjing University of Posts and Telecommunications, Nanjing, China. [2]State Key Laboratory of Flexible Electronics (LoFE) & Institute of Advanced Materials (IAM), School of Flexible Electronics (Future Technologies), Nanjing Tech University (NanjingTech), Nanjing, China. [3]State Key Laboratory of Flexible Electronics (LoFE) & Institute of Flexible Electronics (IFE), Northwestern Polytechnical University, Xi'an, China. ✉e-mail: iamlgu@nwpu.edu.cn; iamzfan@njtech.edu.cn; vc@nwpu.edu.cn

create rigid microenvironments that stabilize triplet excitons. Among these, most strategies have taken the construction of intermolecular interactions (e.g., lp-π and π-π interactions) as their core targets to enhance phosphorescence. Especially, lp-π interactions can promote intersystem crossing rate from singlet to triplet states and provide a rigid molecular environment to stabilize multiple triplet states, thus being more conducive to the improvement of phosphorescent properties[24,25].

Nowadays, ionic bond-mediated room temperature phosphorescence has been reported continually in the form of small molecules, polymers, and host-guest doping[26–30]. The materials constructed by these strategies all utilize strong ionic bonds to restrict the movement of the chromophore, thereby achieving phosphorescence emission[31]. For example, the construction of anion-π interactions promoted the spin-orbit coupling via external heavy atom effect[32], guest molecules significantly affected the arrangement of host molecules for improving phosphorescence efficiency[33], chiral transfer from anionic cellulose derivatives to ionic chromophores for circularly polarized phosphorescence[29] and so forth. In addition, host-guest doping has emerged as a particularly effective and versatile approach due to its straightforward preparation and tunable RTP properties. In this system, guest chromophores are dispersed within a host matrix, where the RTP originates from the guest molecules, while the host matrix provides a rigid microenvironment that suppresses non-radiative decay for achieving RTP. In particular, recent efforts in host-guest RTP materials have primarily focused on optimizing guest chromophores, leading to significant progress. Various functionalized guest molecules have been developed, resulting in RTP materials with ultralong lifetimes, high quantum yields, tunable emission colors, and other desirable properties[26,34–38].

However, not only in ionic host-guest doped systems, but in nearly all molecular doping systems, the reliance on tailored host molecules remains a significant bottleneck. Effective host molecules must exhibit high singlet and triplet energy levels to prevent reverse energy transfer from guest to host and possess compatible molecular configurations and functional groups to establish strong intermolecular interactions. These stringent requirements necessitate precise molecular design and synthesis, hindering the development of universal and high-performance RTP systems. To overcome these limitations, we propose a molecular design strategy for ionic host-guest RTP materials via leveraging consecutive ionic bonds for assembling ionic-bonding networks (Fig. 1). In this approach, non-conjugated alkyl chains serve as the host matrix. These chains naturally possess higher singlet and triplet energy levels than conjugated guest phosphorescent chromophores, effectively preventing reverse energy transfer. Additionally, unlike the weak hydrogen bonding and van der Waals forces commonly observed in traditional host-guest systems, introducing ionic bonds offers excellent advantages[5,39]. Notably, ionic bonds can be harnessed to form rigid ionic-bonding networks between host and guest molecules via electrostatic interactions, providing notable advantages in preventing molecular motion and promoting the external heavy atom effect. Interestingly, most previous studies achieved this effect by directly adding heavy atoms, while this work accomplishes it through the matching of host-guest alkyl chains, demonstrating a different mechanism. Synergizing the rigid ionic network and efficient external heavy atoms effect (Fig. 1b), this design enables the development of high-performance RTP materials with enhanced stability and emission properties. As a result, our system achieves an afterglow lifetime of 572.27 ms at room temperature. Moreover, the universal nature of these host molecules facilitates the creation of RTP materials with tunable emission colors, spanning from blue to red, demonstrating the versatility and broad applicability of this approach. This work introduces an innovative strategy that integrates the strengths of host-guest doping with ionic interactions, providing a universal platform for advancing the field of organic RTP materials. By addressing longstanding challenges in host-guest compatibility and RTP stabilization, this design not only highlights a significant leap forward in material performance but also opens avenues for the practical application of RTP in diverse fields.

Results

To validate our hypothesis, we designed and synthesized a series of quaternary ammonium-functionalized alkyl chain host molecules with varying chain lengths. Additionally, phosphorescent chromophores with different triplet excited-state energy levels were chosen as guest molecules to verify the universality of the strategy. These chromophores were further ionized by trimethylamine to form ionic networks with the ionized host through electrostatic interactions. The chemical structures and purity of guest molecules were fully characterized by nuclear magnetic resonance (NMR), high-resolution mass spectrometry

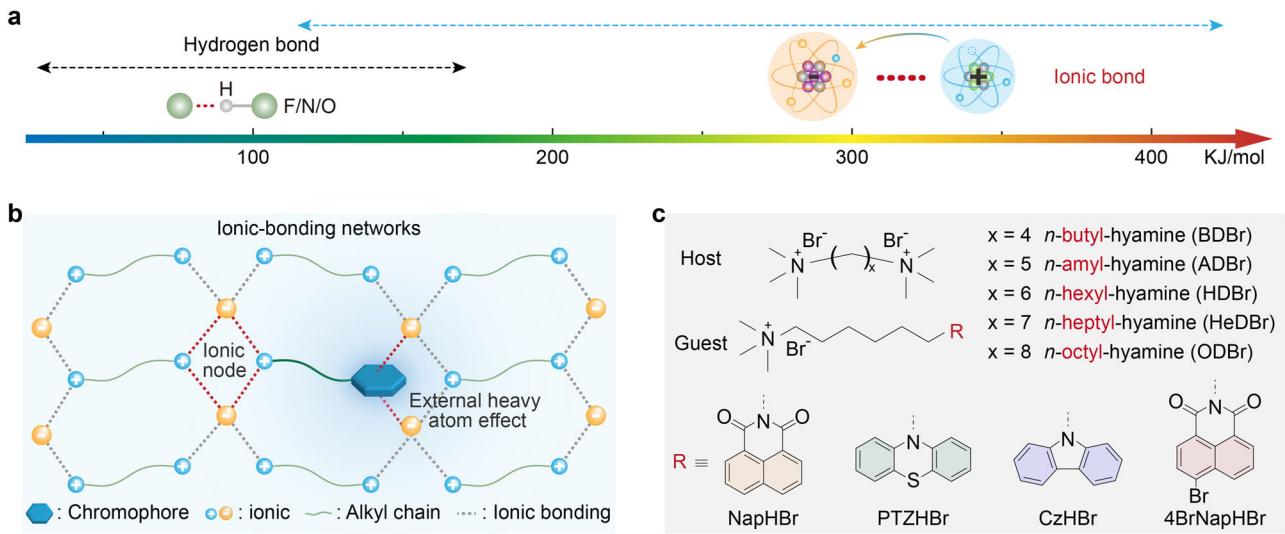

Fig. 1 | Rational design of ionic-bonding network-induced organic room-temperature phosphorescence materials. a Comparison of hydrogen bond and ionic bond. The color change from blue to red indicates an increase in bond energy. **b** Constructing ionic-bonding networks for organic room-temperature phosphorescence composites through quaternary ammonium alkyl chain matching principle in host/guest structures. The ionic nodes and external heavy atom effect can facilitate the phosphorescence emission. **c** Chemical structures of host and guest materials.

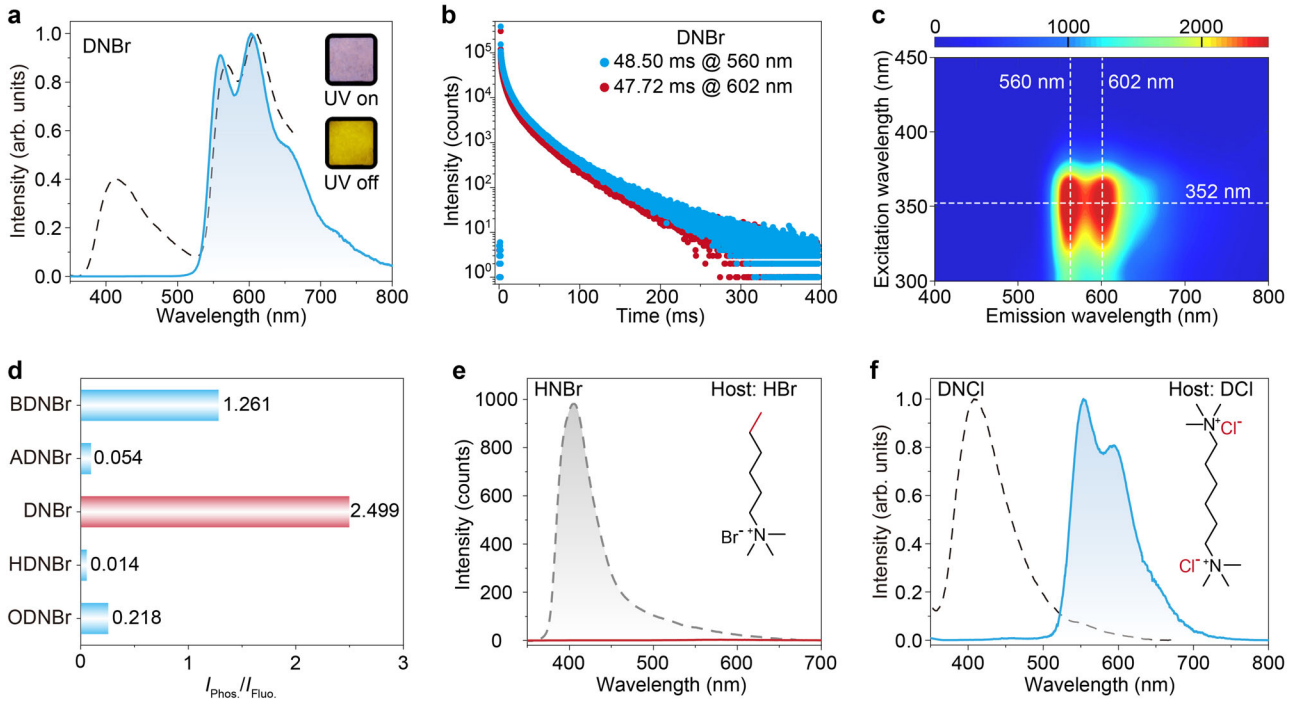

Fig. 2 | Photophysical characterizations of host-guest materials under ambient conditions. a Normalized steady-state photoluminescence (PL, dashed black line) and phosphorescence spectra (solid blue line) of DNBr excited at 340 nm. Inset: Photographs of DNBr, recorded upon switching on (top) and off (bottom) a 365 nm UV lamp. **b** Lifetime decay profiles of phosphorescence emissions. **c** Excitation-phosphorescence mapping of DNBr. The color change from red to blue indicates a decrease in emission intensity. **d** $I_{Phos.}/I_{Fluo.}$ of doped materials with different alkyl chains. **e** Steady-state PL (dashed gray line) and phosphorescence spectra (solid red line) of HNBr excited at 340 nm. Inset: the chemical structure of the host (HBr). **f** Normalized steady-state PL (dashed black line) and phosphorescence spectra (solid blue line) of DNCl excited at 340 nm. Inset: the chemical structure of the host (DCl).

(HRMS), high-performance liquid chromatography (HPLC) and elemental analyses (Supplementary Figs. 6–23 and 25–37). As a proof-of-concept, *n*-hexyl-hyamine (HDBr) and 6-(1,3-dioxo-1H-benzo[de]isoquinolin-2(3H)-yl)-*N*,*N*,*N*-trimethylhexan-1-aminium bromide (NapHBr) were chosen as the host and guest molecules, respectively. The host and guest were dissolved in methanol at a weight ratio of 0.5 wt.%, and the doped material DNBr was prepared by removing the solvent through rotary evaporation. This approach is more straightforward than conventional heating and melting. As expected, upon UV excitation at 365 nm, the DNBr material displayed a yellow afterglow visible to the naked eye for several seconds after the UV light was turned off, demonstrating clear RTP behavior. The photophysical properties of the DNBr were systematically investigated. The steady-state photoluminescence (PL) spectrum revealed dual emission bands at 409, 560, and 602 nm (Fig. 2a). Following an 8 ms delay, only the long-wavelength emission bands at 560 and 602 nm persisted, indicating phosphorescence. The stability was also investigated by monitoring the continuous phosphorescence intensity at 602 nm. As shown in Supplementary Fig. 38, the emission intensity remains unchanged throughout the measurement period under continuous excitation of a 340 nm UV lamp for 1000 s, demonstrating that the DNBr phosphor exhibits excellent UV photostability and is suitable for practical applications under ambient conditions. Then, lifetime decay measurements confirmed the short-wavelength band at 409 nm corresponding to fluorescence with a lifetime of 13.9 ns (Supplementary Fig. 39). In comparison, the long-wavelength bands at 560 nm and 602 nm exhibited lifetimes of 48.50 ms and 47.72 ms, respectively, consistent with phosphorescent emission (Fig. 2b). Analysis of the NapHBr chromophore in dilute solution (1×10^{-5} M) at 77 K showed phosphorescence peaks at 548 nm and 594 nm (Supplementary Fig. 40), aligning closely with the emission bands of DNBr. These results confirm that the yellow RTP originates from the isolated NapHBr chromophore rather than aggregation-induced emission. Notably, only a weak fluorescence band at 364 nm was observed in the spectrum of HDBr, with no detectable phosphorescence under ambient conditions (Supplementary Fig. 41). This indicated that the ionic host primarily functions as a rigid, ionic-bonding network that immobilizes the guest molecules through a confinement effect, without directly participating in or altering their luminescent properties. Excitation wavelength-dependent PL spectra further supported this conclusion, showing consistent emission bands at 560 nm and 602 nm irrespective of the excitation wavelength (300–450 nm), indicating a single stable triplet excited state in DNBr (Fig. 2c). These results suggested that the ionized host molecules can effectively stabilize the triplet excitons of the guest chromophores to achieve phosphorescence at room temperature.

To explore the effect of guest concentration on RTP performance, we prepared host-guest doped materials with guest-to-host weight ratios ranging from 0.1 wt.% to 5.0 wt.%. All samples exhibited yellow afterglows lasting approximately 2 seconds, with phosphorescence lifetimes ranging from 27.85 ms to 48.50 ms. The optimal performance was observed at a guest-to-host weight ratio of 0.5 wt.%, yielding the longest lifetime of 48.50 ms (Supplementary Figs. 42–46). Additionally, the influence of alkyl chain length in the host molecules was investigated by synthesizing a series of host materials (BDBr, ADBr, HDBr, HeDBr, and ODBr) with varying chain lengths (Fig. 1c). Despite differences in chain length, all doped materials (BDNBr, ADNBr, DNBr, HeDNBr, and ODNBr) exhibited fluorescence and phosphorescence dual emission features in their PL spectra, with consistent phosphorescent emission bands at 560 nm and 602 nm (Fig. 2d and Supplementary Figs. 47–51). Notably, DNBr showed the highest phosphorescence-to-fluorescence intensity ratio ($I_{Phos.}/I_{Fluo.}$) of 2.499 and the longest lifetime of 48.5 ms. We hypothesized that this optimal

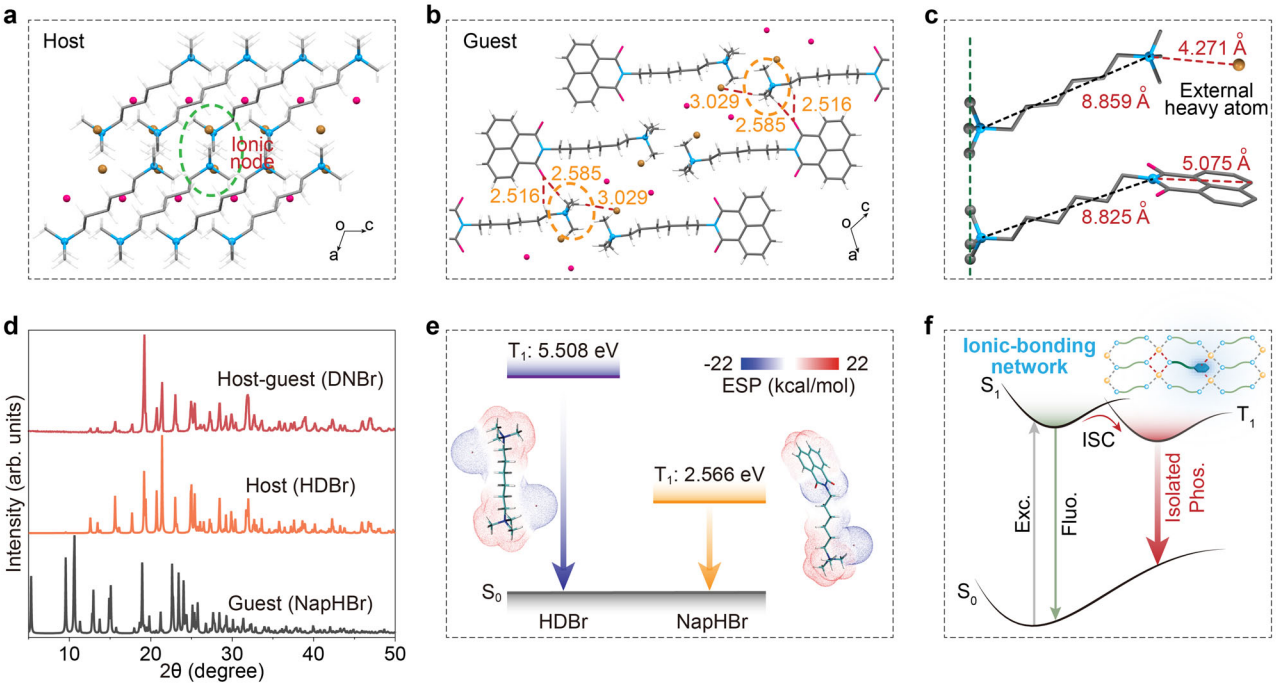

Fig. 3 | Mechanistic investigations of constructing an ionic-bonding network for phosphorescence under ambient conditions. a Molecular stacking of host HDBr. **b** Molecular stacking of guest NapHBr. **c** Alkyl chain lengths of host and guest in crystal structures. Coloured elements: dark grey (C), white (H), pink (O), blue (N) and brown (Br). **d** The X-ray diffraction patterns of DNBr (experimental), HDBr (simulated) and NapHBr (simulated), respectively. **e** The calculated energy levels and electrostatic potentials (ESP) mapped molecular van der Waals surfaces of HDBr and NapHBr, respectively. The color change from blue to red indicates an increase in ESP value. **f** The transition from fluorescence to phosphorescence through the ionic-bonding network.

performance arises from the enhanced self-assembly facilitated by matching the alkyl chain lengths of host and guest molecules, enabling the formation of a rigid ionic network through electrostatic interactions. Moreover, the bromine atoms at the end of the chains of the host molecules might also play a crucial role in accelerating the generation of triplet excitons by virtue of their heavy atom effect. To verify this speculation, we subsequently conducted a set of control experiments. When a non-ionized chromophore (Nap6C) was doped into HDBr, no long-lived RTP was observed, only a fluorescence band at 471 nm, indicating aggregated fluorescence emission due to inefficient self-assembly (Supplementary Figs. 52 and 53). Similarly, when the ionic host was replaced with a non-functionalized alkyl chain host (HBr), intense fluorescence was observed with negligible aggregated phosphorescence under ambient conditions (Fig. 2e and Supplementary Fig. 54). The doped material with non-ionic host and guest structures also exhibited fluorescence without phosphorescence (Supplementary Fig. 55). These control experiments further corroborated the critical role of ionic interactions in constructing a rigid network essential for RTP. Moreover, we also replaced the bromine atoms with chlorine in the host molecule, yielding DNCl. Compared to DNBr, DNCl exhibited decreased phosphorescence intensity in the PL spectrum (Fig. 2f) but significantly prolonged the lifetimes to 214.68 ms and 208.06 ms for the 554 nm and 596 nm emission bands, respectively (Supplementary Fig. 56). To further verify the function of the host material and the great advantages of the ionic-bonding networks, NapHBr was separately doped into various matrices, including classic oligomers and polymers. As shown in Supplementary Fig. 57, when NapHBr is doped into PVA and PEG1000, similar blue emission bands at ~400 nm can be observed in the PL spectra, which ascribes to the fluorescence of the NapHBr chromophores. However, after a delay of 8 ms, a long-wavelength emission band at ~550 nm can only be obtained from the PVA matrix, which originates from the phosphorescence of NapHBr. Whereas when in PEG1000, no phosphorescence was observed. It is worth noting that in the PVA matrix, although the strong intermolecular interactions can induce the appearance of phosphorescent components in the PL spectrum, the $I_{Phos.}/I_{Fluo.}$ value decreased to 0.157 compared with 2.499 in HDBr. These findings highlight the significance of ionic-bonding networks and the heavy-atom effect in enhancing RTP performance. Additionally, enhancement of the rigidity in the host-guest system was also evidenced by conducting decomposition temperature experiments. We found that ionized hosts exhibited a higher decomposition temperature than their non-ionized counterparts (Supplementary Fig. 58). Specifically, for hexylamine, the thermal decomposition temperature increased obviously before and after ionization. This enhancement might be attributed to the formation of strong ionic bonds through electrostatic interactions in the host-guest system. These results suggest that the specific matching rule of alkyl chains between host and guest molecules primarily facilitates the formation of an ordered ionic bond network through electrostatic interactions, thereby enabling effective coordination of external heavy atoms. This promotes the generation and stabilization of triplet excitons, ultimately enhancing room-temperature phosphorescence (RTP).

To further elucidate the mechanism underlying room-temperature phosphorescence in the host-guest doped system, we investigated the molecular arrangements of the host and guest components within the single crystal structures. As illustrated in Fig. 3, the rationale for chain matching lies in its ability to promote the formation of highly ordered ionic-bonding networks that rigidify the microenvironment and sustain long-lived triplet excitons. Specifically, strong ionic interactions among the ionized hosts drive the assembly of a head-to-head cross-linked network, where bromine atoms in the alkyl chains act as ionic nodes to stabilize the structure (Fig. 3a). Furthermore, guest molecules are immobilized by C–H···Br (3.029 Å) and C–H···O (2.516 and 2.585 Å) interactions, which effectively suppress non-radiative motions of the chromophores (Fig. 3b). A critical factor

is the near-perfect length matching of the flexible *n*-hexyl chains between host (8.859 Å) and guest (8.825 Å) molecules (Fig. 3c). This precise alignment enables seamless integration of chromophores into the host's ionic framework, strengthening both ionic-bonding networks and external heavy-atom interactions with Br^- ions.

Subsequently, several control experiments were conducted to verify the roles of ionic-bonding networks. As shown in Supplementary Fig. 59, π−π stacking interactions (3.649 Å) between naphthyl chromophores were observed in the aggregated state. Such stacking could potentially quench the triplet excitons of NapHBr phosphors (Supplementary Figs. 60 and 61)[40], emphasizing the importance of maintaining the ionic network to minimize aggregation-induced quenching. Powder X-ray diffraction (XRD) analysis further confirmed the formation of the ionic network. The experimental XRD pattern of DNBr closely matched the simulated XRD pattern of the HDBr crystal, confirming that the ionic-bonding network remains intact in the DNBr material without being adversely influenced by chromophores' arrangement (Fig. 3d). This suggested that the DNBr microcrystal was formed by embedding guest molecules into host networks. Moreover, the obtained DNBr microcrystals were ground for 10 minutes to prepare DNBr powder. As shown in Supplementary Fig. S62, the PL and phosphorescence spectra of DNBr powder exhibited similar emission peaks compared to DNBr. While the $I_{Phos.}/I_{Fluo.}$ decreased to 0.078 in the PL spectrum of DNBr powder, indicating that grinding destroyed the integration of host and guest. XRD analysis confirmed that the experimental XRD pattern of DNBr microcrystal closely matched the XRD pattern of DNBr powder due to good crystallization of the host (Supplementary Fig. 63). This indicated not only the ionic-bonding networks in the host but also that the assembly between host and guest molecules is crucial in enhancing phosphorescence.

Theoretical simulations supported our design rationale of ionic alkyl chain host and guest molecules. The calculated triplet energy levels for HDBr and NapHBr were 5.508 eV and 2.566 eV, respectively (Fig. 3e). This substantial energy gap indicates that energy transfer does not occur within DNBr, allowing the guest chromophores to independently exhibit RTP. Additionally, the general interaction properties function (GIPF) analysis provided insights into the nature of intermolecular interactions[41]. The quaternary ammonium groups predominantly contributed to the surface area with electrostatic potential (ESP) values between −20 and +20 kcal/mol. Strong negative and positive ESP regions were localized at the electric charge centers, confirming the formation of tightly cross-linked ionic-bonding networks and the confinement of chromophores (Fig. 3f). Moreover, the orbital nature of the states and spin-orbit coupling was investigated in host-guest states based on hybrid quantum mechanics and molecular mechanics (QM/MM) calculations (Supplementary Fig. 64a). It is worth noting that the alkyl chain of the guest molecule all adopted a linear structure in the host-guest doping states with negligible changes in electronic transition characteristics via the analysis of natural transition orbitals (NTOs). This indicated that the alkyl chain of the guest molecule tended to adopt a linear arrangement more readily in the host-guest doping—an arrangement that not only facilitated its insertion into the host structures but also promoted the assembly between host and guest molecules for ionic-bonding networks.

To validate the generality of the strategy, we further selected a series of phosphorescent chromophores with varying triplet excited-state energy levels as guest molecules. By incorporating *n*-hexyl chains via quaternary ammonium functionalization into these chromophores, we synthesized the target guest chromophores, namely 9-(carbazol-9-yl)-*N*,*N*,*N*-trimethylhexan-1-aminium bromide (CzHBr), *N*,*N*,*N*-trimethyl-6-(10H-phenothiazin-10-yl)hexan-1-aminium bromide (PTZHBr), and 6-(6-bromo-1,3-dioxo-1H-benzo[de]isoquinolin-2(3H)-yl)-*N*,*N*,*N*-trimethylhexan-1-aminium bromide (4BrNapHBr). We then doped these guest chromophores into the host of HDBr with a weight ratio of 0.5 wt%. Due to the higher triplet excited-state energy level of the host and the intense ionic bonding between host and guest, the resulting host-guest doped materials exhibited long-lived phosphorescence at room temperature. As illustrated in Fig. 4a, b, the phosphorescence emission bands of the doped materials exhibit a gradual redshift from 444 nm to 620 nm as the triplet excited-state energy levels of the chromophores decrease. This results in a broad color gamut ranging from blue to orange-red phosphorescent emission. Meanwhile, the phosphorescent lifetimes of these host-guest doped materials also showed flexible tunability ranging from 5.87 ms to 572.27 ms (Fig. 4c and Supplementary Table 2). These long-lived phosphorescent emissions all originate from isolated molecular phosphorescence nature (Supplementary Fig. 68). This phenomenon is primarily attributed to the large energy gap between the host and guest molecules, which efficiently prevent reverse energy transfer (Fig. 4d). Furthermore, the significant negative and positive ESPs of the guest chromophores provided an essential prerequisite for constructing a rigid ionic network through electrostatic interactions (Fig. 4d). This network plays a crucial role in suppressing the non-radiative decay of the chromophores, thereby achieving RTP.

Given the cost-effective and readily prepared phosphorescence materials, their potential applications in information encryption were demonstrated by combining mask and squash techniques (Fig. 5a, b). Firstly, DNBr was pressed into a sheet. Upon switching on a 365 nm UV lamp, a blue maple leaf pattern can be observed through a mask (Fig. 5c, top). After cessation of 365 nm lamp excitation, a bright yellow afterglow is visible to the naked eye (Fig. 5c, bottom), which can be utilized for afterglow-based encryption. Additionally, HDBr-host was pressed into a sheet with a "2024" mask. Under 365 nm UV lamp illumination, the sheet exhibited weak fluorescence and no phosphorescence emissions (Fig. 5d, left and middle). However, after treatment with DCzBr solution, intense blue afterglow became observable (Fig. 5d, right). This indicates that the host and guest molecules can rapidly cross-link via electrostatic interactions, endowing the ionic chromophore solution with the functionality of encryption inks.

Discussion

In summary, we proposed a facile and general strategy to construct ionic-bonding networks to prepare organic room temperature phosphorescent doped materials with a long-lived lifetime of up to 572.27 ms. The influences of doped ratios, alkyl chain lengths, and ionic bonding interactions on phosphorescence properties were systematically studied. Notably, the host was suitable for diverse guests by simply attaching ionic groups to chromophores. Taking the experimental and theoretical calculation results, it was found that the matching principle of alkyl chain in host-guest systems was crucial to stabilizing the chromophores through electrostatic interactions and external heavy atom effect. Moreover, the quaternary ammonium groups can cross-link to form ionic nodes in this condition for constructing ionic-bonding networks, thus confining the guest for isolated phosphorescence. These results provide a reference for exploring the mechanism of phosphorescence enhancement by ionic-bonding networks.

Methods

General procedures for synthesis of phosphors

1H-benzo[de]isoquinoline-1,3(2H)-dione (Nap). 1H,3H-benzo[de]isochromene-1,3-dione (1.982 g, 10 mmol) was added into 40 mL ammonium hydroxide (25%). The solution was continually stirred for 8 h at 50 °C. The solvent was removed by rotary evaporation and the residue was purified by column chromatography to yield Nap (1.364 g, 69.2%) as a white solid. ^{1}H NMR (400 MHz, DMSO-d_6): δ 11.62 (s, 1H), 8.37-8.39 (d, 4H), 7.78-7.82 (t, 2H). ^{13}C NMR (DMSO-d_6): δ 164.66, 134.87, 132.11, 130.51, 129.14, 127.62, 123.01.

https://doi.org/10.1038/s41467-026-68468-3

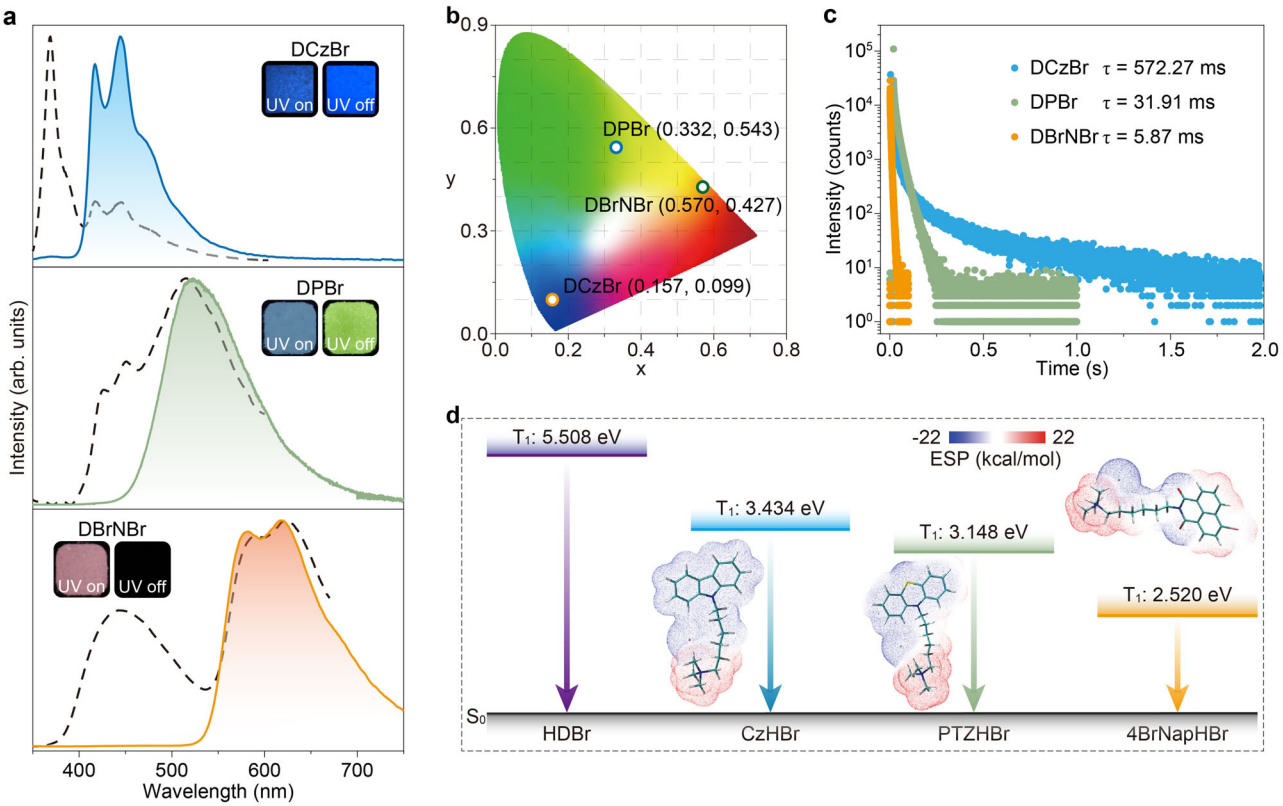

Fig. 4 | Photophysical characterizations of DCzBr, DPBr and DBrNBr under ambient conditions. a Normalized steady-state PL (dashed black line) and phosphorescence spectra (solid line) of DCzBr, DPBr and DBrNBr. Inset: Photographs of DCzBr, DPBr and DBrNBr, recorded upon switching on (left) and off (right) a UV lamp. **b** The CIE color coordinates of DCzBr, DPBr and DBrNBr. **c** Lifetime decay profiles of the phosphorescence emission band at 444, 523 and 620 nm for DCzBr, DPBr, and DBrNBr, respectively. **d** The calculated energy levels and electrostatic potentials (ESP) mapped molecular van der Waals surfaces of CzHBr, PTZHBr and 4BrNapHBr, respectively. The color change from blue to red indicates an increase in ESP value.

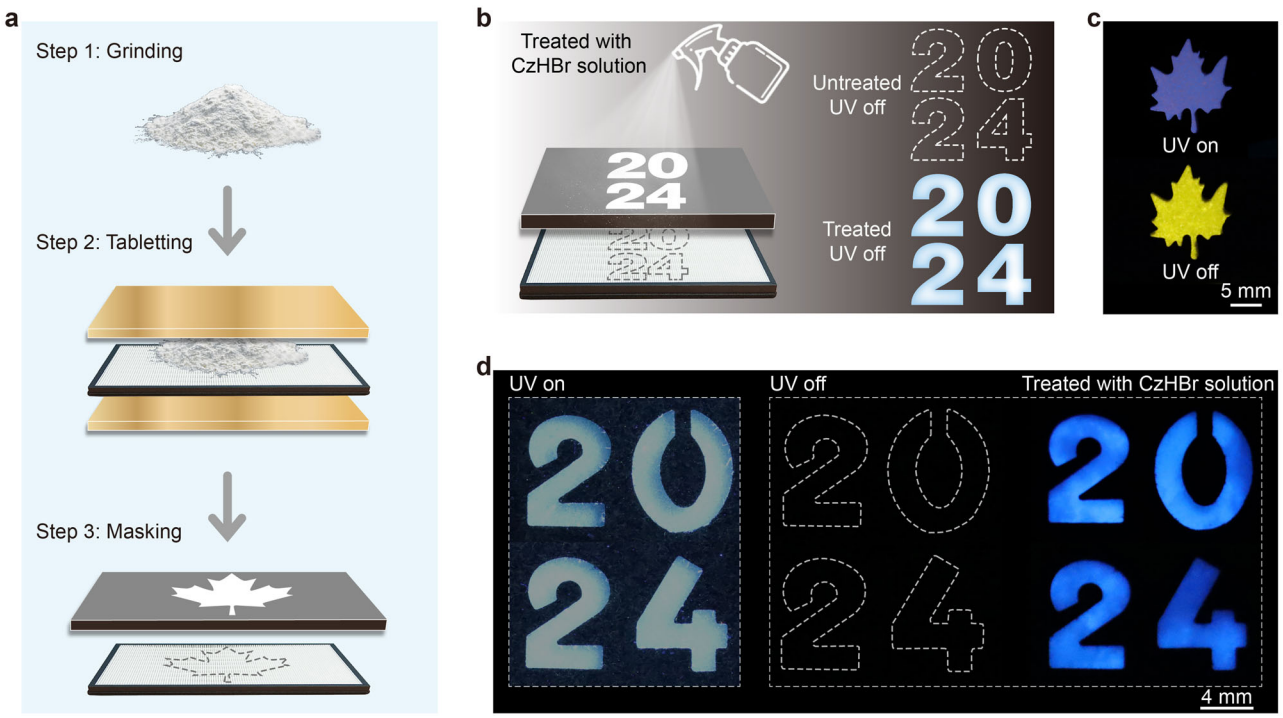

Fig. 5 | Demonstration of phosphorescent doped materials for information encryption under ambient conditions. a Schematic of the pattern-prepared processes. **b** Schematic of the HDBr pattern treated with CzHBr solution. **c** Photographs of a maple leaf pattern with DNBr recorded upon switching on (top) and off (bottom) a 365 nm UV lamp. **d** Photographs of digits with HDBr recorded upon switching on (left) and off (middle and right) a 365 nm UV lamp.

6-bromo-1H-benzo[de]isoquinoline-1,3(2H)-dione (4BrNap). The synthesis of 4BrNap was similar to that of Nap except that 1H,3H-benzo[de]isochromene-1,3-dione was replaced by 6-bromo-1H,3H-benzo[de]isochromene-1,3-dione (2.771 g, 10 mmol). The target molecule 4BrNap was obtained in 67.1% yield (1.853 g). ^{1}H NMR (400 MHz, DMSO-d_6): δ 11.83 (s, 1H), 8.44–8.48 (m, 2H), 8.20–8.22 (d, 1H), 8.13–8.15 (d, 1H), 7.90–7.94 (t, 1H). ^{13}C NMR (DMSO-d_6): δ 164.18, 164.07, 133.15, 131.81, 131.39, 130.76, 130.60, 130.11, 129.69, 129.25, 123.78, 123.01.

2-(6-bromohexyl)–1H-benzo[de]isoquinoline-1,3(2H)-dione (Nap6CBr). Nap (0.394 g, 2 mmol) and NaH (0.240 g, 6 mmol) were added into 30 mL DMF. The solution was stirred for 30 min at 0 °C. Then, 1,6-dibromohexane (1.46 g, 6 mmol) was added to the stirred solution. After that, the solution was continually stirred for 12 h at 90 °C. The solvent was removed by rotary evaporation and the residue was purified by column chromatography to yield NapHBr (0.457 g, 63.5%) as a white solid. ^{1}H NMR (400 MHz, DMSO-d_6): δ 8.40–8.45 (dd, 4H), 7.79–7.84 (q, 2H), 3.97–4.01 (t, 2H), 3.31–3.50 (t, 2H), 1.73–1.80 (p, 2H), 1.56–1.63 (q, 2H), 1.30–1.41 (m, 4H). ^{13}C NMR (DMSO-d_6): δ 163.92, 134.82, 131.81, 131.24, 127.74, 122.57, 35.67, 32.65, 29.50, 27.85, 27.81, 26.17. Analysis (calcd., found for $C_{18}H_{18}BrNO_2$): C (60.01, 60.07), H (5.04, 5.074), N (3.89, 3.80). HRMS (ESI): molecular weight for 360.25, *m/z* found for 360.05903.

2-hexyl-1H-benzo[de]isoquinoline-1,3(2H)-dione (Nap6C). The synthesis of Nap6C was similar to that of Nap6CBr except that 1,6-dibromohexane was replaced by 1-bromohexane (0.990 g, 6 mmol). The target molecule Nap6C was obtained in 47.0% yield (0.264 g). ^{1}H NMR (400 MHz, DMSO-d_6): δ 8.21–8.27 (dd, 4H), 7.64–7.68 (t, 2H), 3.83–3.87 (t, 2H), 1.46–1.50 (p, 2H), 1.17 (s, 6H), 0.72–0.76 (h, 3H). ^{13}C NMR (DMSO-d_6): δ 163.79, 134.73, 131.73, 131.15, 127.65, 122.46, 40.11, 31.48, 27.92, 26.72, 22.51, 14.42. Analysis (calcd., found for $C_{18}H_{19}NO_2$): C (76.84, 76.06), H (6.81, 6.29), N (4.98, 4.82).

4-bromo-2-(6-bromohexyl)–1H-benzo[de]isoquinoline-1,3(2H)-dione (4BrNap6CBr). The synthesis of 4BrNap6CBr was similar to that of Nap6CBr except that Nap was replaced by 4BrNap (0.552 g, 2 mmol). The target molecule 4BrNap6CBr was obtained in 35.9% yield (0.315 g). ^{1}H NMR (400 MHz, DMSO-d_6): δ 8.43–8.48 (m, 2H), 8.22–8.24 (m, 1H), 8.12–8.14 (m, 1H), 7.89–7.93 (m, 1H), 3.94–3.97 (m, 2H), 3.46–3.50 (m, 2H), 1.73–1.80 (p, 2H), 1.55–1.62 (dp, 2H), 1.28–1.43 (m, 4H). ^{13}C NMR (DMSO-d_6): δ 163.35, 163.30, 133.07, 132.06, 131.84, 131.44, 130.24, 129.61, 129.29, 128.74, 123.22, 122.44, 35.66, 32.65, 29.51, 27.80, 27.76, 26.16. Analysis (calcd., found for $C_{18}H_{17}Br_2NO_2$): C (49.23, 50.99), H (3.90, 4.363), N (3.19, 2.90). HRMS (ESI): molecular weight for 439.15, *m/z* found for 437.19311.

10-(6-bromohexyl)–10H-phenothiazine (PTZ6CBr). The synthesis of PTZ6CBr was similar to that of Nap6CBr except that Nap was replaced by phenothiazine (0.398 g, 2 mmol). The target molecule PTZ6CBr was obtained in 32.6% yield (0.236 g). Following the similar synthetic procedure for Nap6CBr, the target molecule PTZ6CBr was obtained (0.236 g, 32.6%). ^{1}H NMR (400 MHz, DMSO-d_6): δ 7.08-7.16 (m, 4H), 6.86-6.95 (m, 4H), 3.77-3.80 (t, 2H), 3.39-3.41 (t, 2H), 1.58-1.71 (dq, 4H), 1.30-1.32 (m, 4H). ^{13}C NMR (DMSO-d_6): δ 145.31, 128.09, 127.65, 124.24, 122.94, 116.33, 46.85, 35.46, 32.69, 27.66, 26.58, 25.82. Analysis (calcd., found for $C_{18}H_{20}BrNS$): C (59.67, 59.84), H (5.56, 5.397), N (3.87, 3.72), S (8.85, 8.442). HRMS (ESI): molecular weight for 362.33, *m/z* found for 362.05674.

9-(6-bromohexyl)–9*H*-carbazole (Cz6CBr). The synthesis of Cz6CBr was similar to that of Nap6CBr except that Nap was replaced by Cz (0.334 g, 2 mmol). The target molecule Cz6CBr was obtained in 63.2% yield (0.417 g). ^{1}H NMR (400 MHz, DMSO-d_6): δ 8.08–8.11 (t, 2H), 7.51–7.55 (t, 2H), 7.37–7.43 (dd, 2H), 7.12–7.17 (dd, 2H), 4.28–4.33 (m, 2H), 3.88–3.40 (d, 2H), 1.60–1.73 (m, 4H), 1.20–1.34 (m, 4H). ^{13}C NMR (DMSO-d_6): δ 140.49, 126.20, 122.56, 120.79, 119.17, 109.72, 42.60, 35.52, 32.66, 28.86, 27.80, 26.12. Analysis (calcd., found for $C_{18}H_{20}BrN$): C (65.46, 66.27), H (6.10, 5.93), N (4.24, 4.11). HRMS (ESI): molecular weight for 330.27, *m/z* found for 330.08490.

NapHBr, 4BrNapHBr, PTZHBr and CzHBr. Nap6CBr, 4BrNap6CBr, PTZ6CBr and CzHBr (1 mmol) were added into 30 mL THF with 5 mL NH_3 (2 mol/L in THF), respectively. The solutions were stirred for 6 h at room temperature. As a result, white target molecules can be obtained after filtering, washing and drying.

NapHBr. ^{1}H NMR (400 MHz, CD_3OD-d_4): 8.51–8.53 (dd, 2H), 8.32–8.34 (dd, 2H), 7.77–7.81 (dd, 2H), 4.12–4.16 (m, 2H), 3.31–3.36 (m, 2H), 3.11 (s, 9H), 1.72–1.85 (ddt, 4H), 1.45–1.53 (m, 4H). ^{13}C NMR (CD_3OD-d_4): δ 163.80, 135.73, 132.18, 130.83, 127.60, 122.30, 66.47, 66.44, 52.16, 39.56, 27.28, 26.07, 25.52, 22.35. Analysis (calcd., found for $C_{21}H_{27}BrN_2O_2$): C (60.15, 59.87), H (6.49, 6.78), N (6.68, 6.39). HRMS (ESI): molecular weight (M-Br) for 339.46, *m/z* found for 339.20641.

4BrNapHBr. ^{1}H NMR (400 MHz, CD_3OD-d_4): δ 8.55 (s, 1H), 8.53–8.54 (d, 1H), 8.30–8.32 (d, 1H), 8.07–8.09 (d, 1H), 7.85–7.89 (dd, 1H), 4.09–4.13 (m, 2H), 3.32-3.36 (m, 2H), 3.12 (s, 9H), 1.71-1.85 (m, 4H), 1.45-1.54 (m, 4H). ^{13}C NMR (CD_3OD-d_4): δ 163.66, 136.01, 132.94, 131.61, 131.17, 130.87, 130.41, 129.76, 128.72, 128.14, 123.15, 122.15, 66.40, 52.18, 39.72, 27.23, 26.07, 25.59, 22.36. Analysis (calcd., found for $C_{21}H_{26}Br_2N_2O_2$): C (50.62, 50.59), H (5.26, 5.57), N (5.62, 5.43). HRMS (ESI): molecular weight (M-Br) for 418.36, *m/z* found for 419.11448.

PTZHBr. ^{1}H NMR (400 MHz, CD_3OD-d_4): δ 7.07–7.17 (m, 4H), 6.87–6.96 (m, 4H), 3.87–3.94 (dt, 2H), 3.19–3.24 (m, 2H), 3.03 (s, 9H), 1.63–1.79 (m, 4H), 1.29–1.53 (m, 4H). ^{13}C NMR (CD_3OD-d_4): δ 145.48, 127.22, 126.99, 125.19, 122.27, 115.70, 66.36, 52.18, 46.32, 26.10, 25.75, 25.47, 22.43. Analysis (calcd., found for $C_{21}H_{29}BrN_2S$): C (59.85, 59.56), H (6.94, 7.21), N (6.65, 6.52), S (7.61, 7.38). HRMS (ESI): molecular weight (M-Br) for 341.54, *m/z* found for 341.20436.

CzHBr. ^{1}H NMR (400 MHz, CD_3OD-d_4): δ 7.20–7.24 (m, 2H), 6.56–6.64 (m, 4H), 6.31–6.36 (m, 2H), 4.06 (s, 9H), 3.42–3.53 (m, 2H), 0.82–1.06 (m, 4H), 0.36–0.57 (m, 6H). ^{13}C NMR (CD_3OD-d_4): δ 139.65, 124.56, 121.90, 118.97, 117.68, 107.79, 51.26, 41.31, 32.16, 27.67, 26.77, 25.48, 21.48. Analysis (calcd., found for $C_{21}H_{29}BrN_2$): C (64.78, 64.85), H (7.51, 7.48), N (7.19, 7.08). HRMS (ESI): molecular weight (M-Br) for 309.48, *m/z* found for 309.23212.

Preparation of doped materials (DNBr, DCzBr, DPBr, DBrNBr)

Taking the host-guest doping ratio of 0.5 wt.% as an example, the guest (NapHBr, 4BrNapHBr, PTZHBr and CzHBr, 2 mg) and host (HDBr, 400 mg) were dissolved in 10 mL CH_3OH. The solution was thoroughly shaken to ensure uniform mixing of the host and guest materials. Then, the solvent was removed by rotary evaporation and the ionic-doped materials were obtained as a white solid.

Reporting summary

Further information on research design is available in the Nature Portfolio Reporting Summary linked to this article.

Data availability

The data of Figs. 2–4 generated in this study are provided in the Source Data file. The data supporting the findings of this study are available within the paper and its Supplementary Information files and are available from the corresponding authors upon request. The X-ray crystallographic coordinates for structures reported in this study have been deposited at the Cambridge Crystallographic Data Centre under

deposition numbers 2242030 and 2242033. These data can be obtained free of charge from the Cambridge Crystallographic Data Centre via www.ccdc.cam.ac.uk/data_request/cif. Source data are provided with this paper.

References

1. Li, Y., Gecevicius, M. & Qiu, J. Long persistent phosphors—from fundamentals to applications. *Chem. Soc. Rev.* **45**, 2090–2136 (2016).
2. Baldo, M. et al. Highly efficient phosphorescent emission from organic electroluminescent devices. *Nature* **395**, 151–154 (1998).
3. Xu, S., Chen, R., Zheng, C. & Huang, W. Excited state modulation for organic afterglow: materials and applications. *Adv. Mater.* **28**, 9920–9940 (2016).
4. An, Z. et al. Stabilizing triplet excited states for ultralong organic phosphorescence. *Nat. Mater.* **14**, 685–690 (2015).
5. Ye, W. et al. Confining isolated chromophores for highly efficient blue phosphorescence. *Nat. Mater.* **20**, 1539–1544 (2021).
6. Peng, X. et al. Purely organic room-temperature phosphorescence molecule for high-performance non-doped organic light-emitting diodes. *Angew. Chem. Int. Ed.* **63**, e202405418 (2024).
7. Shen, S. et al. Edible long-afterglow photoluminescent materials for bioimaging. *Adv. Mater.* **36**, 2404888 (2024).
8. Zhao, W., He, Z. & Tang, B. Z. Room-temperature phosphorescence from organic aggregates. *Nat. Rev. Mater.* **5**, 869–885 (2020).
9. Liu, D. et al. Highly efficient circularly polarized near-infrared phosphorescence in both solution and aggregate. *Nat. Photon.* **18**, 1276–1284 (2024).
10. Li, H., Ma, H., Zhang, P., An, Z. & He, X. Modulating room-temperature phosphorescence of phenothiazine dioxide via external heavy atoms. *Angew. Chem. Int. Ed.* **64**, e202419366 (2025).
11. Ju, H. et al. Polymerization-induced crystallization of dopant molecules: an efficient strategy for room-temperature phosphorescence of hydrogels. *J. Am. Chem. Soc.* **145**, 3763–3773 (2023).
12. Takeda, Y. Modulating the photophysical properties of twisted donor-acceptor-donor π-conjugated molecules: effect of heteroatoms, molecular conformation, and molecular topology. *Acc. Chem. Res.* **57**, 2219–2232 (2024).
13. Wang, H. et al. Abnormal thermally-stimulated dynamic organic phosphorescence. *Nat. Commun.* **15**, 2134 (2024).
14. Deng, Z. et al. Dynamic transition between monomer and excimer phosphorescence in organic near-infrared phosphorescent crystals. *Adv. Mater.* **36**, 2311384 (2024).
15. Dai, W. et al. Halogen bonding: a new platform for achieving multi-stimuli-responsive persistent phosphorescence. *Angew. Chem. Int. Ed.* **61**, e202200236 (2022).
16. Jia, Q. et al. Construction of room temperature phosphorescent materials with ultralong lifetime by in-situ derivation strategy. *Nat. Commun.* **14**, 4146 (2023).
17. Ma, X. & Liu, Y. Supramolecular purely organic room-temperature phosphorescence. *Acc. Chem. Res.* **54**, 3403–3414 (2021).
18. Luo, W. et al. Leveraging multivalent assembly towards high-temperature liquid-phase phosphorescence. *Angew. Chem. Int. Ed.* **64**, e202423650 (2025).
19. Ren, Y. et al. Clusterization-triggered color-tunable room-temperature phosphorescence from 1,4-dihydropyridine-based polymers. *J. Am. Chem. Soc.* **144**, 1361–1369 (2022).
20. Chen, H. et al. Water-resistant organic room-temperature phosphorescence from block copolymers. *Angew. Chem. Int. Ed.* **64**, e202500610 (2025).
21. Garain, S., Garain, B. C., Eswaramoorthy, M., Pati, S. K. & George, S. J. Light-harvesting supramolecular phosphors: highly efficient room temperature phosphorescence in solution and hydrogels. *Angew. Chem. Int. Ed.* **60**, 19720–19724 (2021).
22. Liu, H. et al. Highly efficient blue phosphorescence from pillar-layer MOFs by ligand functionalization. *Adv. Mater.* **34**, 2107612 (2022).
23. Cao, M. et al. Biobased and biodegradable films exhibiting circularly polarized room temperature phosphorescence. *Nat. Commun.* **15**, 2375 (2024).
24. Bhatia, H. & Ray, D. Use of dimeric excited states of the donors in D_4-A systems for accessing white light emission, afterglow, and invisible security ink. *J. Phys. Chem. C.* **123**, 22104–22113 (2019).
25. Bhatia, H., Bhattacharjee, I. & Ray, D. Biluminescence via fluorescence and persistent phosphorescence in amorphous organic donor(D_4)-acceptor(A) conjugates and application in data security protection. *J. Phys. Chem. Lett.* **9**, 3808–3813 (2018).
26. Wang, Y. et al. Organic ionic host-guest phosphor with dual-confined nonradiation for constructing ultrahigh-temperature X-ray scintillator. *J. Am. Chem. Soc.* **147**, 11098–11107 (2025).
27. Sun, J. et al. Enabling controllable time-dependent phosphorescence in carbonized polymer dots based on chromophore excited triplet energy level modulation by ionic bonding. *Angew. Chem. Int. Ed.* **64**, e202415042 (2025).
28. Wang, J., Yang, Y., Zhang, L. & Li, Z. Engineering organic photochromism with photoactivated phosphorescence: multifunctional smart devices and enhanced four-channel data storage. *Adv. Mater.* **37**, 2503074 (2025).
29. You, J. et al. Responsive circularly polarized ultralong room temperature phosphorescence materials with easy-to-scale and chiral-sensing performance. *Nat. Commun.* **15**, 7149 (2024).
30. Yan, Z.-A., Lin, X., Sun, S., Ma, X. & Tian, H. Activating room-temperature phosphorescence of organic luminophores via external heavy-atom effect and rigidity of ionic polymer matrix. *Angew. Chem. Int. Ed.* **60**, 19735–19739 (2021).
31. Dai, W. et al. Recent progress in ion-regulated organic room-temperature phosphorescence. *Chem. Sci.* **15**, 4222–4237 (2024).
32. Wang, J. et al. A facile strategy for realizing room temperature phosphorescence and single molecule white light emission. *Nat. Commun.* **9**, 2963 (2018).
33. Law, A. et al. Sergeant-and-soldier effect in an organic room-temperature phosphorescent host-guest system. *Adv. Mater.* **36**, 2410739 (2024).
34. Hamzehpoor, E. et al. Efficient room-temperature phosphorescence of covalent organic frameworks through covalent halogen doping. *Nat. Chem.* **15**, 83–90 (2023).
35. Ma, H. et al. Boosting organic phosphorescence in adaptive host-guest materials by hyperconjugation. *Nat. Commun.* **15**, 3660 (2024).
36. Zhao, Y. et al. Fused-ring pyrrole-based near-infrared emissive organic RTP material for persistent afterglow bioimaging. *Angew. Chem. Int. Ed.* **63**, e202317431 (2024).
37. Zhao, Z., Zhu, T., Li, A., Zhang, Q. & Yuan, W. Z. Highly efficient red/near-infrared phosphorescence from doped crystals. *Angew. Chem. Int. Ed.* **64**, e202412967 (2025).
38. Lin, F. et al. Fine tuning of hydrogen bonding interaction on boosting the room-temperature phosphorescence in organic host-guest system. *J. Phys. Chem. Lett.* **16**, 1916–1923 (2025).
39. Ye, W. et al. High-performance circularly polarized phosphorescence by confining isolated chromophores with chiral counterions. *Adv. Mater.* **36**, 2410073 (2024).
40. Sternlicht, H., Nieman, G. & Robinson, G. Triplet-triplet annihilation and delayed fluorescence in molecular aggregates. *J. Chem. Phys.* **38**, 1326–1335 (1963).
41. Murray, J. S. & Politzer, P. The electrostatic potential: an overview. *Comp. Mol. Sci.* **1**, 153–163 (2011).

Acknowledgements

This work is supported by the National Natural Science Foundation of China (Grant No. 22505114, 22475098, 62288102, 22475172, 22275085, and T2441002), the Basic Research Program of Jiangsu (Grant No. BK20243057, BK20250678), the Natural Science Foundation of the

Jiangsu Higher Education Institutions of China (Grant No. 24KJB430028, 25KJA430009), and Natural Science Research Start-up Foundation of Recruiting Talents of Nanjing University of Posts and Telecommunications (Grant No. NY224035).

Author contributions

W.Y., L.G., Z.A. and W.H. conceived the experiments and wrote the paper. W.Y., C.H., Y.L., Y.G., Z.M. and H.S. were primarily responsible for the experiments. W.Y. and Y.L. performed the lifetime measurements. W.Y. conducted the single-crystal measurement and analysis. A.L. and H.M. contributed to TD-DFT calculations. All authors contributed to the data analyses.

Competing interests

The authors declare no competing interests.

Additional information

Supplementary information The online version contains supplementary material available at https://doi.org/10.1038/s41467-026-68468-3.

Correspondence and requests for materials should be addressed to Long Gu, Zhongfu An or Wei Huang.

Peer review information *Nature Communications* thanks the anonymous reviewers for their contribution to the peer review of this work. A peer review file is available.